J Solid State Electrochem (2006) 10: 929–933
DOI 10.1007/s10008-005-0039-1

ORIGINAL PAPER

Peizhi Shen · Yudai Huang · Lang Liu · Dianzeng Jia
Zaiping Guo

Synthesis and electrochemical performance of $LiCr_xMn_{2-x}O_4$ (x=0,0.02,0.05,0.08,0.10) powders by ultrasonic coprecipitation

Received: 24 January 2005 / Revised: 4 June 2005 / Accepted: 14 June 2005 / Published online: 2 August 2005

Abstract $LiCr_xMn_{2-x}O_4$($x=0$, 0.02, 0.05, 0.08, 0.10) compounds with a spinel crystal structure have been prepared by a novel ultrasonic co-precipitation method. The effects of the calcination temperature and the citric acid-to-metal ion molar ratio (R) on powder characteristics and electrochemical performance are evaluated. It is found that the optimum R and sintering temperature for $LiCr_xMn_{2-x}O_4$ materials by the ultrasonic co-precipitation method are $R=5/6$ and 800°C, respectively. The calcined powders are loosely bound agglomerates of abnormally coarsened particles with a narrow range of particle sizes. The effect of Cr doping was also explored. Electrochemical studies show that optimum materials synthesized by the ultrasonic co-precipitation method demonstrate good cycling performance.

Keywords Ultrasonic · Coprecipitation · Lithium-ion battery · Cathode

Introduction

Lithium-ion batteries are the state-of-the-art power sources for consumer electronics, primarily because of their high specific energy and volumetric energy density. Lithium cobalt oxide ($LiCoO_2$) and similar lithium-transition metal oxides ($LiNiO_2$, $LiNi_{0.2}Co_{0.8}O_2$) are intercalation compounds that are used as lithium-storage materials in rechargeable lithium-ion batteries. Lithium Manganese oxide ($LiMn_2O_4$) has also been studied extensively as a potential cathode material for lithium rechargeable batteries due to its low cost, low toxicity and high energy density. Despite its impressive improvement over previous $LiMn_2O_4$ materials, the cycling performance of $LiMn_2O_4$ needs to be further improved in order to meet commercial requirements. A very effective way for improving the cycling performance of $LiMn_2O_4$ is to synthesize divalent or trivalent ion doped $LiM_xMn_{2-x}O_4$ spinel phase (M = Al, Mg, Co, Ni, Fe, Ti, Zn and Cr, etc.).

It is well known that the quality of the $LiMn_2O_4$ powders depends on the synthetic method and the precursors used. Preparation conditions determine the physical and chemical properties of the $LiMn_2O_4$ materials, such as particle size, lattice parameters, stoichiometry and average Mn valence. In general, $LiMn_2O_4$ powders have been prepared via a solid-state reaction by sintering lithium and manganese salts at low (400–500°C) [1, 2] or high (700–900°C) temperature [3–5]. This process requires a long sintering time, extended grinding and has also several other disadvantages: inhomogeneity, irregular morphology, large average particle size with broad particle size distribution, and poor control of stoichiometry. In recent years, "soft-chemical" methods have been widely used to synthesize the desired powders, e.g. sol-gel [6–8], the tartaric acid or citric acid gel process [9], the Pechini process [10], and the electrochemical process [11]. Additionally, co-precipitation synthesis of $LiMn_2O_4$ is an attractive method, but is often hindered by the high solubility of lithium salts in water [12–14].

In this study, a new ultrasonic co-precipitation method is employed in the preparation of $LiCr_xMn_{2-x}O_4$ (x=0,0.02,0.05,0.08,0.10). Here the chromium ion is used as a doping cation to improve the cycling performance of $LiMn_2O_4$. An ultrasonic bath is used in order to obtain good stoichiometric control of $LiCr_xMn_{2-x}O_4$ spinel with uniform particle size distribution.

P. Shen · Y. Huang · L. Liu · D. Jia (✉)
Institute of Applied Chemistry, Xinjiang University,
Urumqi, 830046 People's Republic of China
E-mail: jdz@xju.edu.cn
Tel.: +86-991-8583265
Fax: +86-991-8581006

Z. Guo
Institute for Superconducting Electronic Materials,
University of Wollongong, Wollongong,
NSW, 2522 Australia

Experimental

All reagents were analytically pure and were used without further treatment. Experimental details are as follows.

The preparation of $LiCr_xMn_{2-x}O_4$ ($x = 0,0.02,0.05,0.08,0.10$)

Stoichiometric lithium acetate, manganese acetate, chromic nitrate and citric acid, with citric acid-to- metal ion molar ratios (R) = 1, 5/6, 2/3 and 1/2, respectively, were completely dissolved in 40 ml distilled water. The solution was then treated in an ultrasonic bath for 8 to 10 min. The cream-like precipitate was first dried at 120°C to remove water, and then decomposed at 400°C for 1 h. The mixture obtained was ground and then calcined in air at various temperatures (650–850°C) for 10 h in a muffle furnace.

Materials characterization

The thermal decomposition behavior of the precursor was examined by means of thermogravimetry and differential thermal analysis (TG-DTA; NETZSCH STA449C, Germany). An X-ray diffractometer (XRD; MAX MXP18AHF, Japan) using Cu Kα radiation was used to characterize microstructures of the samples. The morphological characteristics of the product were examined using scanning electron microscopy (SEM; LEO 1430VP, Germany).

Electrochemical measurements

The electrochemical cells consisted of a $LiCr_xMn_{2-x}O_4$-based composite as the positive electrode, a Li disk as the negative electrode, and an electrolyte of 1M $LiPF_6$ in a 1:1 (volume ratio) mixture of ethylene carbonate (EC)/dimethyl carbonate (DMC). The cathodes were made by dispersing 85% active materials, 10% acetylene carbon black and 5% polyvinylidene fluoride (PVDF) in a solvent of N-methyl-pyrrolidone (NMP). The slurry was then coated on aluminum foils by using a blade. The loading of active material was about 6 mg cm^{-2}. The film was dried at 60°C in air for 2 h and then was vacuum dried at 120°C for 3 h. Celgard 2400 membrane was used as the separator. The cells were assembled in an argon-filled glove box. A Li metal disk served as counter electrode in the 2-electrode setup. Cyclic voltammetry (CV) experiments were carried out over the voltage range of 3.0–4.35 V at a scan rate of 0.1 mV s^{-1}. Charge-discharge tests were performed on battery test instrument (KINGNUO CT2001A, China) at a constant current density of 0.30 mA cm^{-2} within the potential range of 3.0–4.35 V. All the electrochemical tests were carried out at room temperature.

Results and discussion

The preparation of precursor is the most crucial step in the synthesis procedure. First, metal acetates and citric acid are dissolved in water, forming a sol with the metal-chelating citric acid. Then, the sol coagulates, and precipitation is induced after ultrasonication. This technique ensures the uniform mixing of raw materials and leads to a short production time for the $LiCr_xMn_{2-x}O_4$ compounds. It was found that the sintering temperature, the citric acid-to- metal ion molar ratios (R) and the Cr doping level influence the microstructure and the morphology of $LiCr_xMn_{2-x}O_4$ compounds and thereby lead to changes in the electrochemical performance. In this study, experiments were first designed to search for an optimum sintering temperature and R value, which would result in the best cycling performance for lithium intercalation/deintercalation. In these experiments, pure $LiMn_2O_4$ was chosen as an example.

Thermal analysis was first carried out to determine the optimum heat-treatment temperature of the precursor. TGA/DTA analysis on the precursors with $R = 1$ was conducted at a heating rate of 10°C min^{-1} in air. The TGA/DTA curves shows that the decomposition of the precursor mainly occurs below 400°C. The weight loss between 400 and 700°C is less than 0.05%. The DTA curve in Fig. 1 shows a large exothermic peak at about 370°C, which might be due to the decomposition of the organic groups and the formation of spinel $LiMn_2O_4$. Therefore, a preheating temperature of 400°C was chosen in our experiment.

The preheated samples were then sintered at higher temperature to obtain products with better crystallization and purity. Figure 2 shows the XRD patterns of the $LiMn_2O_4$ calcined at various temperatures with $R = 1$ and that of the samples calcined at 800°C with different R. For the sample calcined at 650°C, besides the spinel $LiMn_2O_4$ crystalline phase, several minor peaks, which correspond to the presence of Mn_2O_3, were also ob-

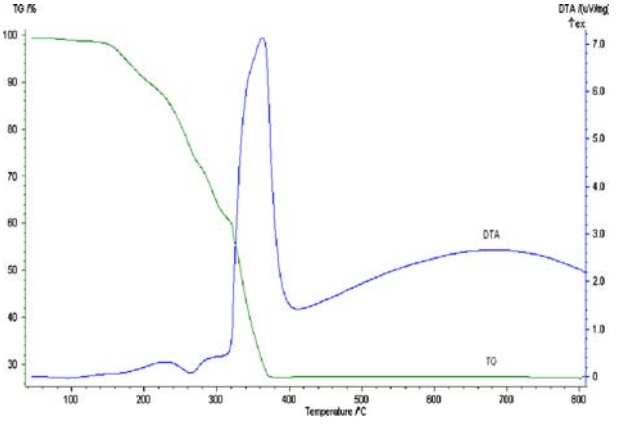

Fig. 1 The TG/DTA trace of precursor heat-treated from room temperature to 800°C at a heating rate of 10°C min^{-1} in air

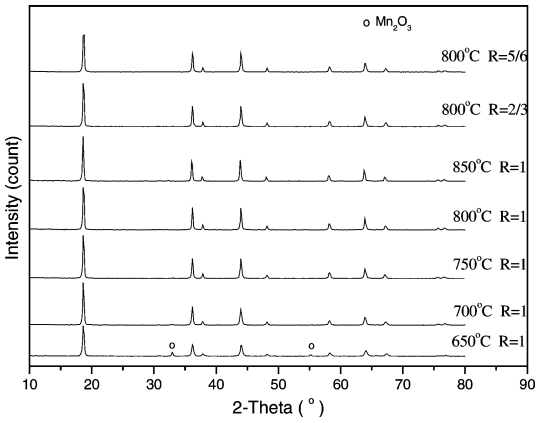

Fig. 2 The XRD patterns of $LiMn_2O_4$ powders calcined at various temperatures and $LiMn_2O_4$ with different R calcined at 800°C

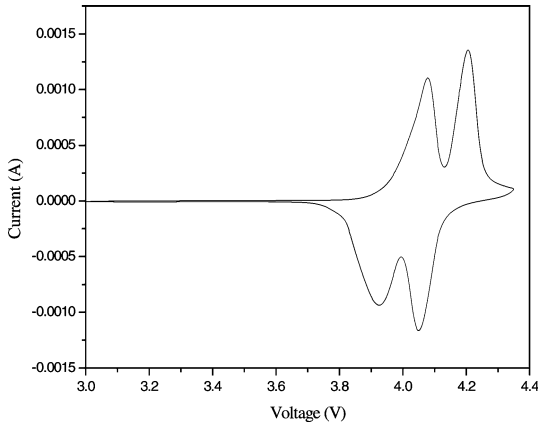

Fig. 4 The cyclic voltammogram of the second cycle for the $LiMn_2O_4$ fired at 800°C with $R=1$. Scan rate is 0.1 mV s^{-1}

served. The impurity phase completely disappeared after the sample was calcined at or above 700°C. Compared with the $LiMn_2O_4$ prepared by ultrasonic co-precipitation with $R=1$ calcined at 650°C, the XRD peaks of $LiMn_2O_4$ calcined at higher temperature become remarkably sharper, indicating better crystallization. The XRD patterns of samples calcined at 800°C for 10 h with different R values (1, 5/6 and 2/3) are also shown in Fig. 2. Single-phase spinels are observed in all samples. When R decreased to 1/2, no precipitation occurred during sonication. The single-phase spinel is of the Fd3m space group in which the lithium ions occupy the tetrahedral (8a) sites and manganese resides at the octahedral (16d) sites [15].

Figure 3 shows the scanning electron micrographs of samples calcined at various temperatures in air for 10 h with $R=1$. It can be seen that calcined powders are loosely bound agglomerates of abnormally coarsened particles. The particle size distribution is apparently narrow and the average is in the submicrometer range. The particle size shows no obvious changes with increasing sintering temperature.

Figure 4 shows the cyclic voltammogram of a $LiMn_2O_4$ electrode in 1 M $LiPF_6$, 1:1 EC/DMC solution in the potential region of 3.0–4.35 V at sweep rate of 0.1 mV s^{-1}, and Fig. 5 presents the charge/discharge characteristics of $LiMn_2O_4$ in the second cycle corresponding to Fig. 4. The cell was cycled at 0.30 mA cm^{-2}

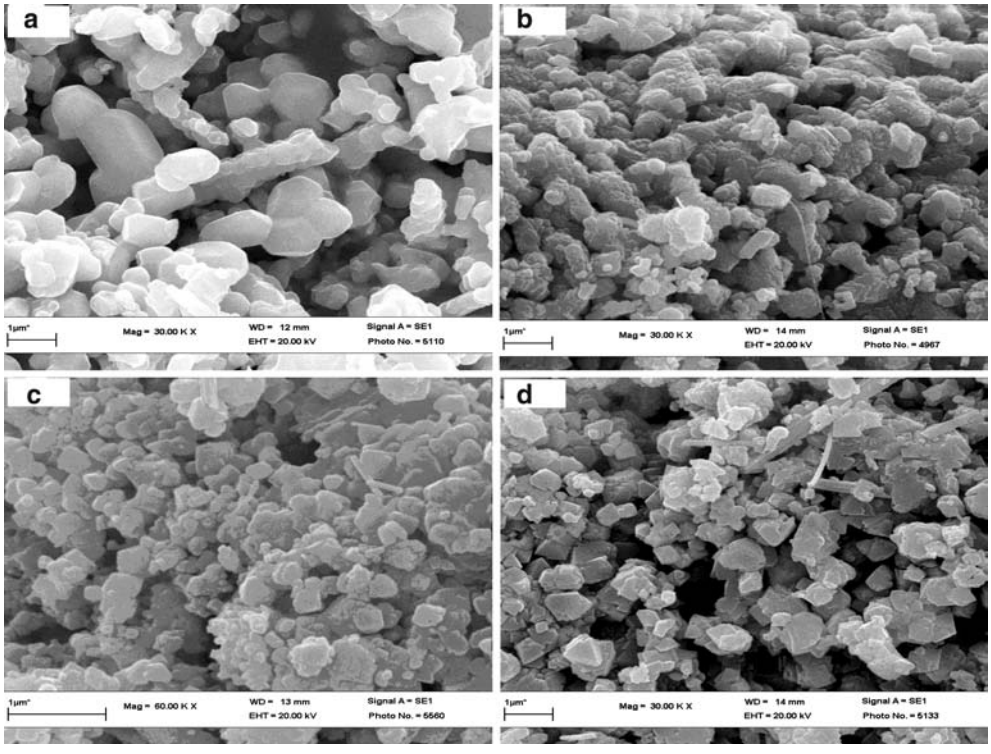

Fig. 3 Scanning electron micrographs of the $LiMn_2O_4$ with $R=1$calcined at **a** 700°C **b** 750°C **c** 800°C **d** 850°C

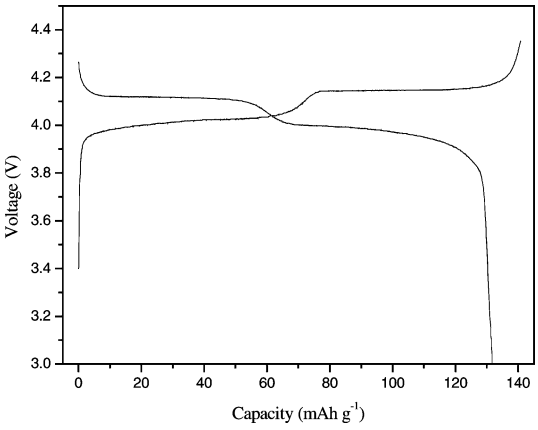

Fig. 5 The second cycle charge/discharge curves for the $LiMn_2O_4$ powder calcined at 800°C with $R=1$ at current rate 0.3 mA cm^{-2}

between 3.0 V and 4.35 V. Two pairs of redox current peaks were observed in Fig. 4. They correspond to a two-step reversible intercalation reaction in which the lithium ions occupy tetragonal 8a sites in spinel $Li_xMn_2O_4$ ($x<1$) in two steps [16]. Correspondingly, two potential plateaus located at 3.9 and 4.1 V, respectively, were observed in the charging/discharging curves. These plateau potentials are in good agreement with the peak potentials in Fig. 4. The upper plateau region of the discharge curve represents a two-phase equilibrium between λ-MnO_2 and $Li_{0.5}Mn_2O_4$, whereas the second plateau represents a phase equilibrium between $Li_{0.5}Mn_2O_4$ and $LiMn_2O_4$ [17, 18].

Figure 6 compares the discharge capacity vs. cycle number of the Li/ $LiMn_2O_4$ cell for powders calcined at different temperatures with $R=1$. The cells were cycled up to the 30th cycle at a rate of 0.3 mA cm^{-2} between 3.0 and 4.35 V. The single-phase $LiMn_2O_4$ sintered at 800°C demonstrates excellent cycling performance. It initially delivered 131.7 mA h g^{-1} and retained 126.1 mA h g^{-1} at the 10th cycle and 116.8 mA h g^{-1} at the 30th cycle, which is better than that of the powders sintered at other temperatures.

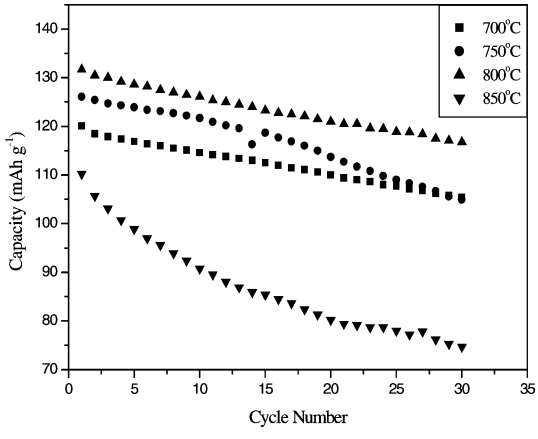

Fig. 6 Specific discharge capacity of $LiMn_2O_4$ fired at different temperatures, where $R=1$

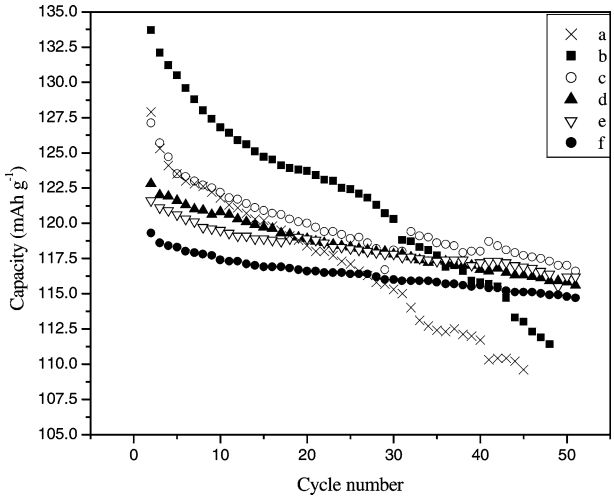

Fig. 7 Cycling performance of $LiMn_2O_4$ with various R and $LiCr_xMn_{2-x}O_4$ with $R=5/6$ calcined at 800°C: **a** $LiMn_2O_4$ with $R=2/3$, **b** $LiMn_2O_4$ with $R=5/6$, *c* $LiCr_{0.02}Mn_{1.98}O_4$, **d** $LiCr_{0.05}Mn_{1.95}O_4$, **e** $LiCr_{0.08}Mn_{1.92}O_4$, **f** $LiCr_{0.10}Mn_{1.90}O_4$

The influence of the citric acid-to-metal ion molar ratio (R) on the electrochemical performance of products was also investigated to determine the ideal conditions for preparing $LiMn_2O_4$ with the best electrochemical characteristics. Figure 7 shows the discharge capacity vs. cycle number of the Li/ $LiMn_2O_4$ cell for powders with different R calcined at 800°C. The $LiMn_2O_4$ powders with $R=5/6$ delivered a initial discharge capacity of 133.7 mA h g^{-1} and retained 120.3 mA h g^{-1} at the 30th cycle and 112.3 mA h g^{-1} at the 45th cycle, which is better than that of $R=2/3$ or $R=1$ (see Fig. 6). Based on the discussion above, it can be concluded that the optimum R and sintering temperature for $LiMn_2O_4$ materials produced by the ultrasonic co-precipitation method are $R=5/6$ and 800°C, respectively.

To further improve the cycling stability of $LiMn_2O_4$ system, studies on a series of Cr-doped $LiMn_2O_4$ were performed. Fig. 7b–f show a comparison of the initial discharge characteristics of $LiCr_xMn_{2-x}O_4$ ($x=0$, 0.02, 0.05, 0.08, 0.10) calcined at 800°C for 10 h with $R=5/6$. As the Cr content increases, the initial capacity decreases slightly. The initial discharge capacity decreases from 133.7 to 119.3 mA h g^{-1}, as the Cr content increases from $x=0$–0.10. However, the capacity fading with cycling is significantly decreased with increasing Cr content. The discharge capacity retentions for $LiMn_2O_4$, $LiCr_{0.02}Mn_{1.98}O_4$,$LiCr_{0.05}Mn_{1.95}O_4$,$LiCr_{0.08}Mn_{1.92}O_4$ and $LiCr_{0.1}Mn_{1.90}O_4$ after 45 cycles are 83.9, 91.7, 94.6, 96.1, and 96.5% of their initial discharging capacity, respectively. According to initial discharge capacity and discharge capacity retention, the optimum Cr content is 0.08. The good cyclability is mainly due to an increase in the stability of the spinel structure. The radius of Cr^{3+} (0.615 Å) is near to that of Mn^{3+} (0.68 Å), and it exists in a stable d^3 configuration where it prefers an octahedral coordination [19–21]. Therefore, $LiCr_xMn_{2-x}O_4$ is

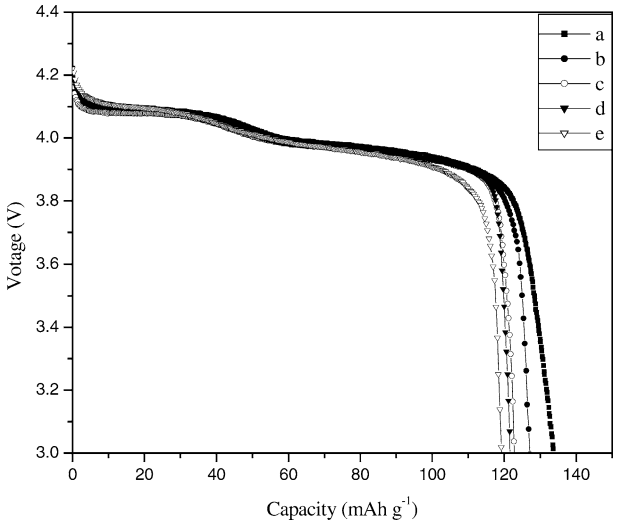

Fig. 8 Discharge behavior at the first cycle of $LiCr_xMn_{2-x}O_4$: **a** $x = 0.00$, **b** $x = 0.02$, **c** $x = 0.05$, **d** $x = 0.08$, **e** $x = 0.10$

still a single-phase spinel. During the lithium intercalation and de-intercalation process, the cubic symmetry of this spinel is not destroyed, thus its cycling behavior has been greatly improved. The substitution of some Mn-O bonds in the spinel with Cr–O may also enhance the stability of the octahedral sites in the spinel skeleton structure [22]. Consequently, the stability of spinel structure is improved, thus the dissolution of Mn^{3+} can be suppressed [23] (Fig. 8).

Conclusions

We have successfully synthesized $LiCr_xMn_{2-x}O_4$ ($x = 0$, 0.02, 0.05, 0.08, 0.10) by a new method we have named ultrasonic co-precipitation. All of the as-prepared $LiMn_2O_4$ powders were identified as a single spinel phase. $LiMn_2O_4$ annealed at 800°C with $R = 5/6$ delivered a high discharge capacity as well as good capacity retention. As Mn was replaced by Cr, the initial capacity decreased slightly, but the capacity retention was enhanced. The initial discharge capacity of $LiCr_{0.08}Mn_{1.92}O_4$ is 121.6 mA h g^{-1} and it retained 116.8 mA h g^{-1} at the 45th cycle. Therefore, it can be seen that ultrasonic co-precipitation is an effective method to prepare cathode material for lithium-ion batteries with a simple process that only requires a short reaction time.

Acknowledgements This work was financially supported by the Natural Science Foundation of China (no. 20366005, 20462007).

References

1. Ye SH, Lv JY, Gao XP, Wu F, Song DY (2004) Electrochim Acta 49:1623
2. Tang XC, He LP, Chen ZZ, Jia DZ, Xia X (2003) Chem J Chin Univ 24:576
3. Hunter James C (1981) J Solid State Chem 39:142
4. Ohzuku T, Kitagawa M, Hirai T (1990) J Electrochem Soc 137:769
5. Guo ZP, Ahn JH, Liu HK and Dou SX (2004) J Nanosci Nanotech 4:162
6. Yang W, Liu Q, Qiu W, Lu S, Yang L (1999) Solid State Ionics 121:79
7. Hwang BJ, Santhanam R, Liu DG, (2001) J Power Souces 101:86
8. Liu H, Wu YP, Rahm E, Holze R, Wu HQ (2004) J Solid State Electrochem 8:450
9. Hon YM, Fung KZ, Lin SP, Hon MH (2002) J Solid State Chem 163:231
10. Liu W, Farrington GC, Chaput F, Dunn B (1996) J Electrochem Soc 143:879
11. Hill LI, Portal R, Verbaere A, Guyomard D (2001) Electrochem Solid State Lett 4:A180
12. Qiu XP, Sun XG, Shen WC, Chen NP (1997) Solid State Ionics 93:335
13. Naghash AR, Lee JY (2000) J Power Sources 85:284
14. Chan HW, Duh JG, Sheen SR (2003) J Power Sources 115:110
15. Wakihara M (2001) Mat Sci Eng R 33:109
16. Miura K, Yamada A, Tanaka M (1996) Electrochim Acta 41:249
17. Ohzuku T, Kitagawa M, Hirai T (1991) J Electrochem Soc 137:769
18. Wang GG, Wang JM, Mao WK, Shao HB, Zhang JQ, Cao CN (2004) J Solid State Electrochem DOI 10.1007/s10008-004-0607-9
19. Robertson AD, Lu SH, Averill WF, Howard WF Jr (1997) J Electrochem Soc 144:3500
20. Robertson AD, Lu SH, Howard WF Jr (1997) J Electrochem Soc 144:3505
21. Li GH, Ikuta H, Uchita T, Wakihara M (1996) J Electrochem Soc 143:178
22. Oikawa K, Kamiyama T, Izumi F, Nakazato D, Ikuta H, Wakihara M (1999) J Solid State Chem 146:322
23. Wu YP, Rahm E, Holze R (2002) Electrochim Acta 47:3491